OPTIMIZATION OF A PHOTOCATALYTIC CHEMICAL REACTOR FOR CARBON DIOXIDE REDUCTION

A Thesis

Presented to the Faculty of the Graduate School

of Cornell University

In Partial Fulfillment of the Requirements for the Degree of

Master of Science

by

Yuval Kaminer

MAY 2019

ABSTRACT

Climate change challenge is mainly driven by anthropogenic Carbon Dioxide emissions that worsen the greenhouse effect, which can be mitigated, in part, by the help of the photocatalytic chemical reactor for CO_2 reduction presented in this work. A chemical reduction of the Carbon Dioxide in the presence of Hydrogen gas could create products like Carbon monoxide and water, also referred to as the reverse water gas shift reaction (RWGS), which can possibly be re-used for industrial needs. This work presents how using an innovative chemical reactor that helps emit light onto a novel photocatalyst, can create both high Carbon Dioxide reduction percentile and overall products flow with reduced energy requirements; It will demonstrate the optimization process, through numerical simulations, using the COMSOL Multiphysics program, and related lab experiments with a 0.1 L lab scale reactor, for the RWGS reaction. The work described in this paper takes into account that the technology used needs to show both theoretical and practical feasibility in order to scale up easily to industrial size.

By Yuval Kaminer

BIOGRAPHICAL SKETCH

Yuval Kaminer finished his B.Sc. in Mechanical Engineering and graduated from the Technion institute of technology, located in Haifa Israel, in 2016. After graduating, he worked in the defense industry as a material properties researcher and a mechanical design engineer, before coming to the United states of America to pursue a Master of Science in Mechanical engineering at Cornell University.

This work is dedicated to my wife, Carmel, who has given me the two greatest presents in life: Mattan Emanuel and Yael Rebecca.

ACKNOWLEDGEMENTS

This work has been made possible with the greatly appreciated help of my advisor, Professor David Erickson. Another considerable contribution for the progress and understanding of this project has been thanks to the help of my committee member, Dr. Tobias Hanrath. Finally, without the determination, hard work and endless hours of the doctoral candidate Mr. Xiangkun (Elvis) Cao, this work could not cross the finish line. Lastly, thank all the rest of the Erickson Lab group that have made this process manageable.

I thank you all.

TABLE OF CONTENTS

LIST OF TABLES

LIST OF FIGURES

LIST OF SYMBOLS

A_f	Arrhenius equation - Frequency factor / pre-exponential factor
E_a	Arrhenius equation - Activation energy
R	Gas constant
K_{eq}	Chemical reaction constant
P_{in}	Light power input, per guiding rod total surface.

LIST OF ABBREVIATIONS

WGS	Water Gas Shift
RWGS	Reverse Water Gas shift
GC	Gas Chromatograph
MFC	Mass Flow Controllers
UV-LED	Ultra Violate Light Emitting Diodes
CO_2	Carbon Dioxide
CO	Carbon Monoxide
GHG	Greenhouse Gas
Au-STO	Gold Strontium Titanite ($SrTiO_3$; STO)
CO-STO	Cobalt STO
$In_2O_{3-x}(OH)_y$	Indium Oxide
$Bi_zIn_{2-z}O_{3-x}(OH)_y$	Bismuth doped Indium Oxide

INTRODUCTION

1.1 Carbon Mitigation

Climate change is a major global concern due to the possible encompassing impact it might have on world population, current life style, society advancement, flora and fauna [1]. Potential climate change hazards include rising sea levels, increase in extreme weather events (such as severe winter storms), increase in hurricanes and longer and harder draughts. Climate change must be addressed and treated for its' cause and not it's symptoms [2]. It is claimed that the biggest contributor to climate change is anthropogenic Carbon Dioxide emission that worsen the greenhouse effect. Global emissions are on the rise, despite the increase in renewable energy sources, mainly because of exponential increase in energy demand, especially in developing countries. Despite the shift to renewable energy sources from fossil fuels in the developed world, in developing countries, which experience the greatest rise in energy demand, new renewable sources cannot reach the demanded increase [3]. On top of that, most of the developed world, still uses fossil fuels as its main energy source, and the shift to a completely carbon emission free economy is still unreachable. Consequently, carbon mitigation, capture and reprocess (e.g. CCS) technologies are the only solution to stop and maybe reverse the greenhouse effect and thus the climate change [4].

Due to estimations of increased emissions in the developing world in the near future and the hardship of reducing carbon emissions in the developed world in necessary amounts, technological actions of carbon mitigation, CCS, will have to be made in order to fight the strengthening of the greenhouse effect. Some proposed actions are more naturally aspired in character, such as increasing soil's carbon capture by planting more trees or certain crops, others are more direct, such as CO_2 filtration from the air and storing it in designated places. Nonetheless, Carbon mitigation should be addressed from multiple directions simultaneously, with every known technology and for any existing carbon emitting source.

The subject of efficiently transforming Carbon dioxide reduction into useful product, such as Carbon Monoxide, is a heavily researched area [5] ; especially reductions were CO is the main product. Since CO is a useful gas for many other industrial purposes, and also enjoys a high selectivity for many catalysts, it can make a good research comparison tool [6][7][8][9].

The two main reduction pathways are either electrocatalysis or photocatalysis. Although on both pathways large amount of research has been done [10], no definite conclusion has surfaced about the higher efficiency or economic viability of one over the other [11]. Catalyst selection and design for the

RWGS through photocatalysis is one of two major challenges in CO_2 reduction [12]. Second challenge is light integration into the reactor for the photocatalytic process [13], since chemical reactors are usually designed for high temperatures and high pressures which usually covered by a steel structure [14]. One less optimal solution to the light integration problem is optical fibers which allow high surface ratio for light dispersion, but lead to a problematic light source coupling [15].

This research work takes an already published nanostructure-photocatalyst by the Ozin's group [16] [17], and investigates whether the help of an innovative reactor that uses simple and novel light coupling from the external source to the catalyst, could improve conversion and achieve "best in class" results [18]. This Thesis describes a set of experiments that proposes a novel approach to mitigate carbon emissions from gas power plants. By capturing flue gas from the power station's smoke stacks, running its separated CO_2 component through a photocatalytic chemical reactor, and converting it in into other useful gasses that could be later used in the industry, High efficiency carbon mitigation could be achieved.

1.2 Experimental work

The first part of this paper describes the major experimental steps taken in the empiric work on Carbon Dioxide reduction with an innovative photochemical reactor [19]. The work included testing of different phases of the reactor that were changed during an optimization process throughout the research and experience-based practical knowledge gathered. While the experimental work started independently and mostly progressed unimpeded, as the research continued to evolve, simulations and numerical calculations became an integral part of the work by optimizing operational conditions and geometrical structure. For example: changing the number and orientation of the baffles, or manipulating experimental conditions, such as flow rates, in order to get a higher chemical retention time inside the reactor, and thus higher conversion.

1.3 Simulations

The second part of this Thesis describes the numerical optimization process for the photo-chemical reactor on fluid dynamics and photocatalytic chemical reaction using COMSOL Multiphysics. The experiments are simulated using several different numerical modules, chemical reaction numerical calculation, Transport of diluted species, laminar flow, heat transfer and a Multiphysics coupler. This work starts with the very basic calibration of chemical

simulations going through several intermediate steps until the final version, attempting to accurately simulate the real lab-experiments. Starting from a one-dimensional structure for chemical reaction, moving through two-dimensional model to calibrate a simplified case of the entire process and finally a three-dimensional model to best describe real conditions. The majority of the project is self-reliant, since documented simulations of chemical reactors are abundant [20] [21] [22], even some on RWGS [23], simulations of photocatalytic reactions inside a chemical reactor is absent.

The prosses of optimizing the chemical reaction was done by comparing reactor's product output gas based on concentration amounts. Optimized parameters are directly linked to the flow mixing optimization and the photocatalytic behavior by optimizing both surface reaction and light distribution in the reactor. The final product was a series of normalized graphs, each presenting the normalized output products as a function of a specific parametric change.

While the simulations section of this paper, is an integral part of the experimental work, it is presented independently because of the simulations' ability to reproduce results for untested experimental conditions. Conditions as new internal structures for reactor designs and unavailable boundary conditions, that are either untested empirically or future planned, are good

examples for parameters which can't be efficiently checked in current lab settings and therefore the simulations, once calibrated, are the best tool for predictions and optimization. Since most simulation work is theoretical and only partly tested, it is disconnected from the actual lab work, hence un-dependent.

EXPERIMENTAL SETUP

2.1 Introduction

The following chapter describes the experimental work to study, learn and optimize light introduction to a chemical reactor. Enhancing photocatalytic reaction with improved light integration is the main novelty in this innovative chemical reactor design, which tested a number of different photochemical catalysts to improve the chemical reaction of Carbon Dioxide reduction. The major improvement in the proposed reactor is the ability to introduce light, along the entire length of the reactor with high efficiency flux through the photocatalyst. Light introduction was done with the use of guide rods that were coated with different novel photochemical catalysts, which helped promote Carbon Dioxide redox process through photocatalysis-reduction process. The large scale of the described chemical reactor is another additional attribute of this experimental setup, in an attempt to prove the scalability of the project.

2.2 First design

The first form of the design was using easily customizable parts in order to create an easy to build and modify reactor for various initial tests. The chemical reactor, as seen in Figure 2.2-1, was expected to run on high

pressures and high temperatures, while also keeping working regime and being inert in the chemical reaction. Using Swagelok® products was chosen because of the versatility of existing offered and used components. The first iteration of the reactor was made by two 'T' shaped Yor-Lok 1-inch fittings, made from Zink plated steel, connected to each other by a piece of 1 inch 316 stainless steel. On the two sides of the Yor-Lok fittings were two 1-Inch NPT lime-glass sight windows to create an overall volume of 0.1 Liter.

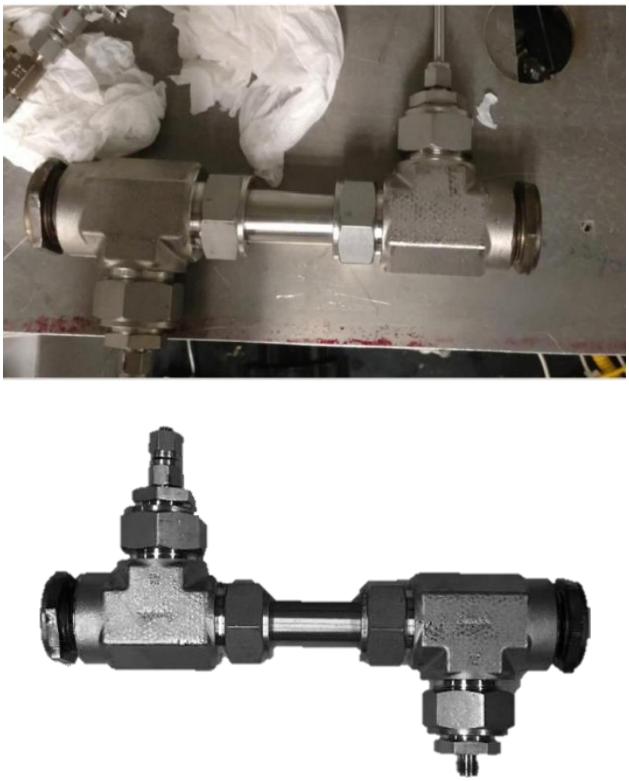

Figure 2.2-1 First iteration of the reactor with Swagelok components and fused glass endings.

On each of the two 'T' fittings final (third) ports, diameter reducers were connected to allow input and output lines to connect. On the input side a

pressure gauge and a 316 stainless steel pressure relief disc component, that raptures if pressure exceeds 350 psi to ensure working safety by avoiding explosions caused due to pressure buildup. The outlet side comprised of two output valves, the first pointing out into the hood to have a controlled release of gasses while flushing the reactor between runs with Nitrogen. The other output valve is connected to a water collector and then to the gas chromatograph (GC) device for products analysis. Water collector is used because the GC device is generally not designed to large quantities of water such as were predicted in the reactions.

The core innovation of this simple reactor design is to allow maximum external light penetration into the chemical reactor, promoting photocatalysis, while granting the ability to have high pressure high temperature as working conditions. Light introduction into the reactor was promoted by two main components, the first, the side sight windows on the two opposing sides of the reactor and the second, thin internal fused quartz light guidance rods.

Each of the two light coupling components serve a dual purpose. The Rayotek sight windows that were placed on the two opposing sides of the reactor allowed the light from two ultraviolet light emitting diodes (UV-LED) to enter the chemical reactor for the desired photocatalytic reaction. The second purpose is to help guide more thermal energy from the concentrated sunlight,

as planned in later phases of the project, thus increasing the reaction equilibrium towards the products. While the project started with white light LED, it quickly changed to shorter wavelength, higher energy, UV LEDs to help increase the photocatalytic effect for the same experimental conditions, boosting the output products. The two roles the light rods serve are an easy coupling mechanism for the introduced light at the windows, allowing a more homogenous diffusion of the light throughout the length of the reactor. The rods also serve as a large surface bed for the photo-catalyst throughout the reactor, thus even increasing the efficiency of light scattering on the catalyst surface inside the reactor and the active contact surface for reactants-catalyst interaction.

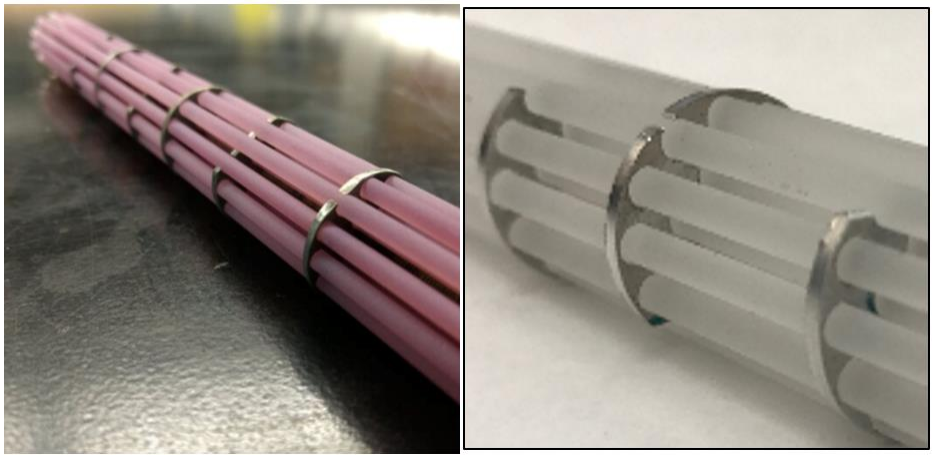

Figure 2.2-2 – Flow baffles holding the light guiding rods with two types of photocatalyst, Au-STO on the left and $In_2O_{3-x}(OH)_y$.

Another component that serves with dual purpose is the flow baffles, seen in Figure 2.2-2, with a main purpose of holding the light guiding rods in a uniform spread across the reactor cross section, while also serving as a static mixing structures for the gas flows. This improved flow efficiency will be later discussed in the simulation chapter.

This configuration showed promising results on the first phase of experiments but also surfaced some critical design flaws that were later addressed and will be discussed in the next section. These changes allowed for a more efficient chemical reaction and a photocatalytic improving affect to be presented more clearly.

2.3 Reactor optimization

During the research operations of the reactor, several design iterations were made, either to improve process optimization, fix physical boundary

conditions or make the operation of the reactor easier and more robust. Some small changes were made instantaneously during operations, such as the distance, orientation and number of baffles, or experimental conditions like temperature or flows; other changes like general reactor design required larger effort and even a complete reactor redesign that happened later in the experimental process. These changes are specified along with the rationale behind each change and the results on conditions and outputs.

Figure 2.3-1 - Fused quartz 1" sight windows. Curtesy of Rayotek company [24].

2.4 Design iterations

First immediate change, that was made early in the process, was changing the fused soda-lime glass sight windows as seen in Figure 2.3-1, that were meant to allows the penetration of light into the rector, to fused Quartz. This change was due to the fact that Quartz is transparent to Ultra-Violet wavelength, depicted in Figure 2.4-1, unlike the borosilicate or the soda-lime glasses, which have partial or no transmissivity to UV wavelengths.

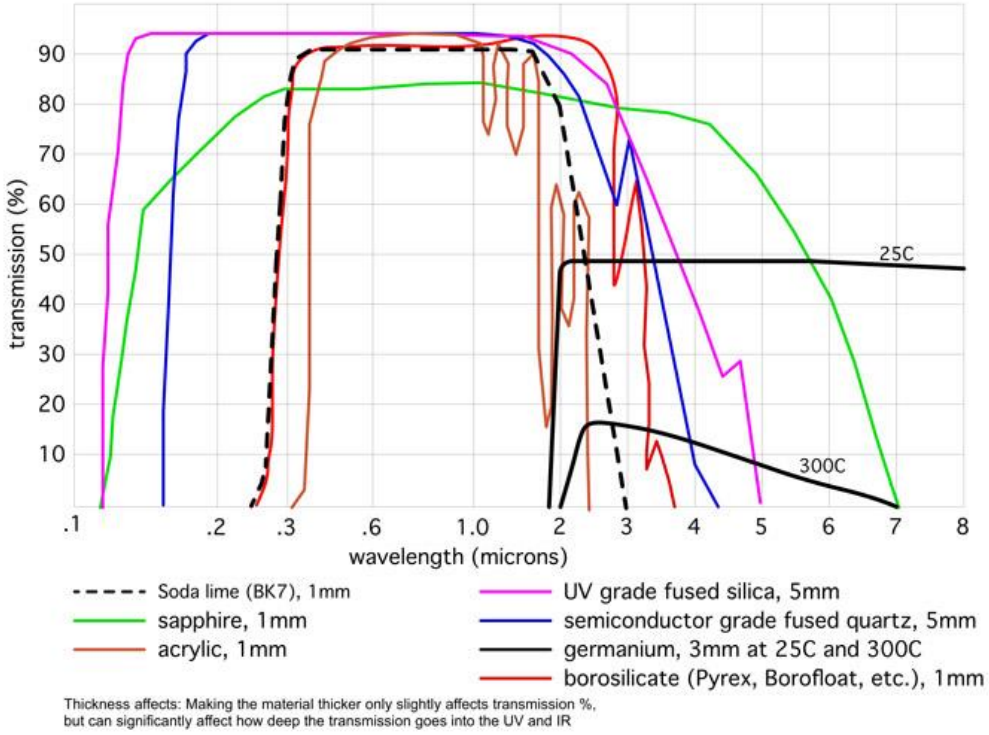

Figure 2.4-1 - Transmission curves for commonly used types of glass in industrial purposes. Curtesy of Rayotek company [25].

This change was a necessary once, because of the decision to use mostly light in the UV wavelength (under 400 Nm) seen in Figure 2.4-2 as violate color, rather than a white LED light that covers the entire visible spectrum (400-700 Nm).

Figure 2.4-2 - Visible end of the emitted light from a UV LED seen in violate color, pointed into the chemical reactor during experimental operation.

The next step was replacing the sight windows completely with a flanged configuration, visible on **Error! Reference source not found.**.

Figure 2.4-3 - Main reactor body with threaded flange configuration at each end for better and easier operation.

Each reactor Swagelok 'T' connector' was fitted with a threaded flange followed by a 2" diameter quartz disc with a thickness of 0.5", that serves as the glass port for the light to enter the reactor, that is held in place with the help of a second flange and a set of circumference bolts. A couple of heat resistant elastic gaskets were placed on each side of the quartz window, to serve as a gas seal on the glass while reducing stress on it by the steel flange tightening of the steel flanges directly to the glass, by serving as a mild damper as seen in Figure 2.4-4.

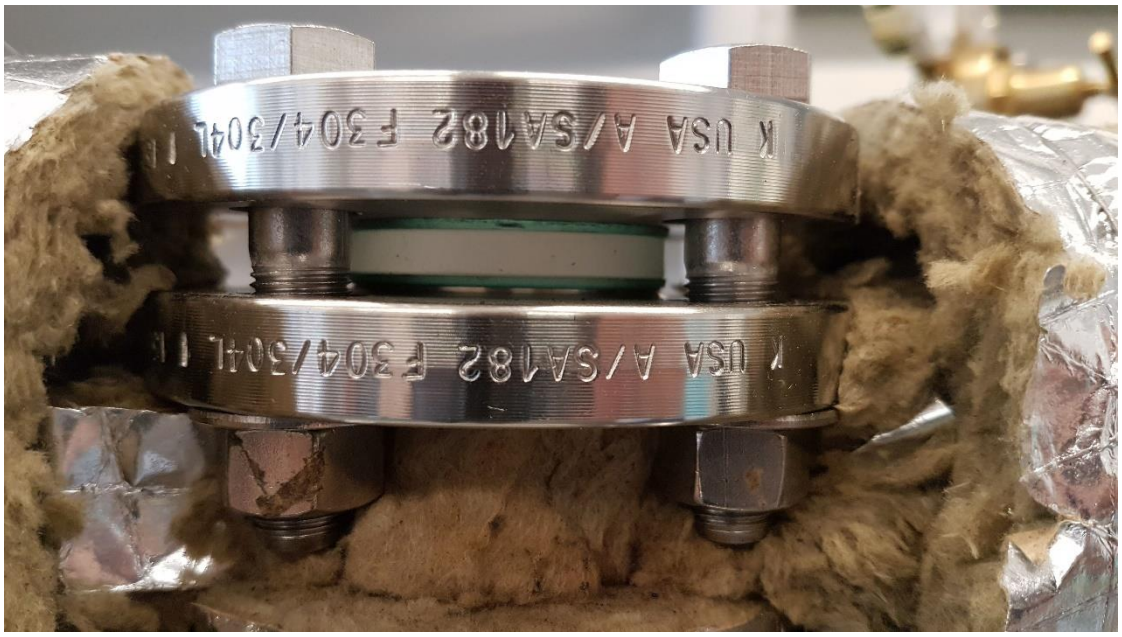

Figure 2.4-4 - Flange structural set-up with the bottom threaded flange connected to the reactor's body, followed by a set of gasket-quartz plate-gasket and secured by a second flange.

Changing to flanges from the sight windows allowed for easy access into the reactor for maintenance work, e.g. replacing the light guiding rods with catalyst. Except ease of access, flange configuration also helped eliminating reoccurring leakage that originated from the 1" NPT threading that was the connection for the sight window.

Figure 2.4-5 - Latest reactor configuration based on CFD optimization and ease of operation.

The latest reactor change in design was moving to a costume design structure, made from simple 1" welded tubes, with flange endings on all ports, Figure 2.4-5. The new reactor included two main changes from previous design, that were based on optimization conclusions from previous experiments series and a CFD flow optimization simulations that were done on a COMSOL Multiphysics model (elaborated on Chapter 4). The main modification is switching from a Swagelok component-based configuration to a costume welded pipe structure with flange ports configuration, this decision was made to allow easy and fast access to the input output ports, outside the isolation layer, as well as easy and configurable connectivity.

The second modification was moving the input output ports of the reactor as close as possible to the reactor ends in order to utilize the maximum available volume and reduce dead volumes at the end of each side that have fewer mixing flows with the middle part of the reactor. This last part is presented more elaborately in Chapter 4 on the 2D model section.

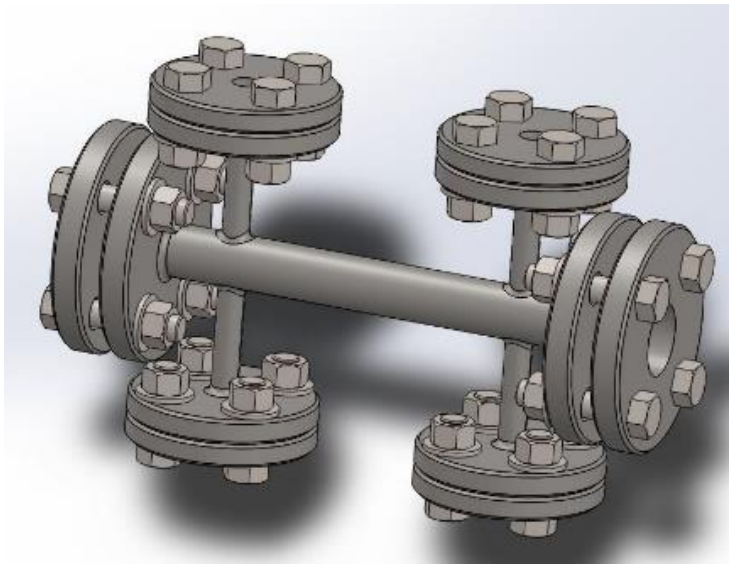

Figure 2.4-6 - CAD model of the costume reactor for manufacturing.

2.5 Photocatalyst

The first studied catalyst in the research process was Gold nanoparticles on the surface of Strontium Oxide (Au-STO) followed by the use of Co-STO. Both catalysts presented significant photocatalytic characteristics from added light into the reaction, despite that change, the overall amounts of conversion and relative CO_2 conversion produced from these catalysts were not as good in comparison to other reported catalysts from literature. Another challenge

that occurred during experiments, was that while going above 350ºC for increased reaction conversion, instead of increasing, the reaction started decreasing, mainly due to catalyst deactivation and Carbon deposition on the rod's catalyst surface. That additional fact further pushed the research to look for other catalytic compounds.

The next and current catalyst that is researched is a duel configuration Indium-Oxide, $In_2O_{3-x}(OH)_y$, with a second configuration that is doped with small amounts of Bismuth, $Bi_zIn2_{-z}O_{3-x}(OH)_y$. This catalyst was chosen due to high reported conversion rates and intense photocatalytic effects, based on the work of Ozin et al [26].

2.6 Experimental conditions

The goal of this research was to identify optimal reaction parameters for maximum Carbon Dioxide reduction. Many different initial conditions were chosen to experimentally identify the optimal state of the reactor reaction, such as different temperatures, input flows, source light intensity etc.

These parameters have several different limitations, such as a maximum reaction temperature. Catalyst deactivation which is the limiting factor for reaction temperature, as in the case of $In_2O_{3-x}(OH)_y$ which was reported to start losing reaction capabilities from as early as 200ºC, with increased

deactivation above 350ºC, which was chosen as the maximum reaction temperature that was eventually chosen for most experiments due to highest percentile and absolute conversions. In order to optimize for the temperature while getting a comparable result to other published results, experiments ran through the full spectrum of temperatures for every 50ºC from 0 to 350ºC.

Other input parameters were examined over different steps over the entire range, such as the light source that was checked between 0 and 100 [W], maximum availability of the light source. Gas input flows were also checked over the entire possible span, starting in the lowest measurable input flows and limited by the mass flow controllers on the high end.

2.7 Experimental results

This section describes the best current results by experiments. While other previous work on this reactor presented good and promising results that can lead to further research directions. Eventually, due to time and effort and different catalyst degradation constraints, best identified reactor conditions were 350ºC for maximum available conversion amounts, with 15 [W] input from the power source and 2 $\frac{ml}{min}$ of each of the reactants.

The above conditions were empirically chosen optimum. For example, the temperature is the highest possible to run enough time to produce stable

results before catalyst degradation. Light source power was identified as a production optimum, that below and above produce less conversion, and the flow rates were the lowest measurable, but also enabling longest possible reaction time, due to low flow rate.

One limiting factor for the experiments is the thermal equilibrium which dictates the maximum conversion available for specific temperature, which is calculated from the theoretical thermal equilibrium, Figure 2.7-1, of the regular WGS and is reversed from that reaction. Every result that we've got, never reached steady state higher than thermal equilibrium conversion rates.

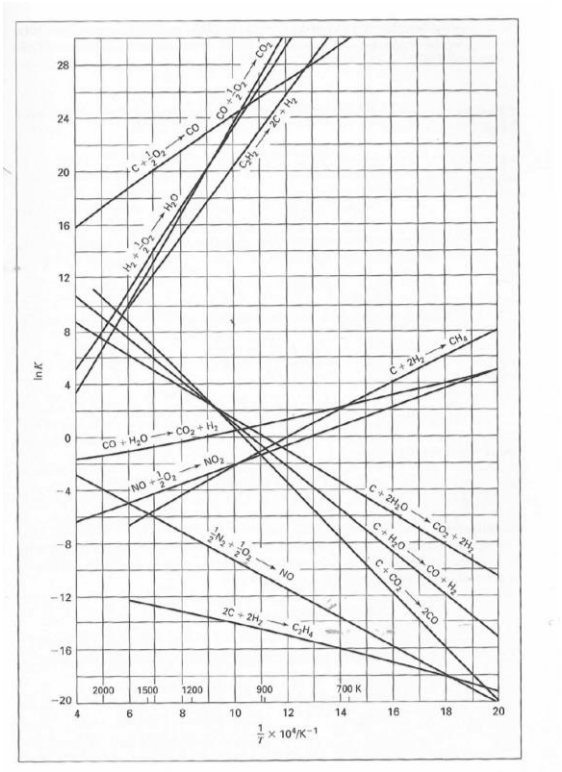

Figure 2.7-1 - Equilibrium constants as a function of temperature [27].

Calculating the equilibrium value for 350°C which corresponds to $16 \cdot 10^{-4}[\frac{1}{K}]$ leads to $lnK \cong 3$ or for the RWGS $lnK_{RWGS} = \frac{1}{lnK_{WGS}} \cong \frac{1}{3}$, Which in turn equals to concentration ratio of products and reactants:

$$K_{RWGS} = \frac{[Y_{CO}][Y_{H_2O}]}{[Y_{CO2}][Y_{H_2}]} = \frac{\zeta \cdot \zeta}{(1-\zeta)(1-\zeta)} = \frac{1}{3}$$

$$\zeta = \frac{0.36}{2} \cong 0.18 = [Y_{CO}] = [Y_{H_2O}]$$

That calculation leads to the theoretical equilibrium and Carbon conversion of ~18% in 350°C.

Typical results of a lab experiment are presented in Figure 2.7-2, as the CO percentile amount as a function of time. The percentile amounts are for a reaction with the starting conditions of 2 $\frac{ml}{min}$, that started at 300°C until reaching equilibrium and then transitioning to 350°C, around 13:30, followed by a turning on the light source, around 17:00. It is visible that for every step in the way, CO concentration amounts changed dramatically.

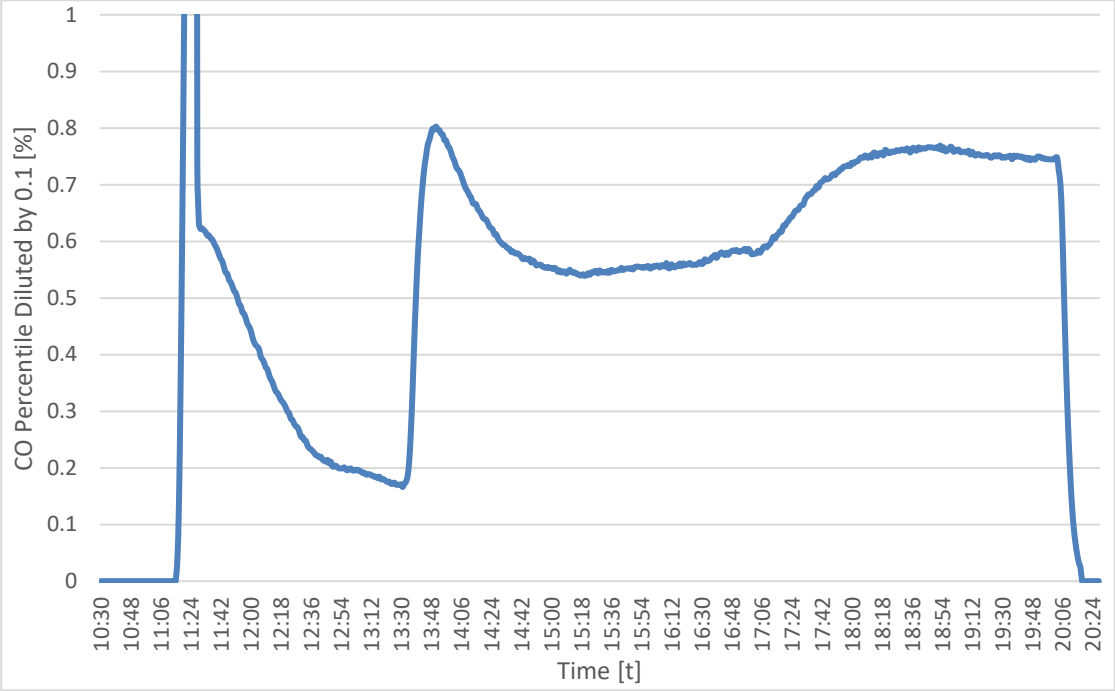

Figure 2.7-2 - CO concentration as a function of time and changing experimental conditions.

After a certain increase of temperature or prolonging reactor running time, thus increasing the reaction time, catalyst degradation was starting to appear as a reduction in products, such as CO concentration. That decrease could be explained by two reasons. First, temperature degradation that is caused in high temperatures due to catalyst damage. Second, Carbon depositions on the light guiding rods that blocks out both active catalyst and photochemical enhancing scattered light, this second reason could be seen clearly in Figure 2.7-3, in a comparison of a used rods formation, next to an unused batch.

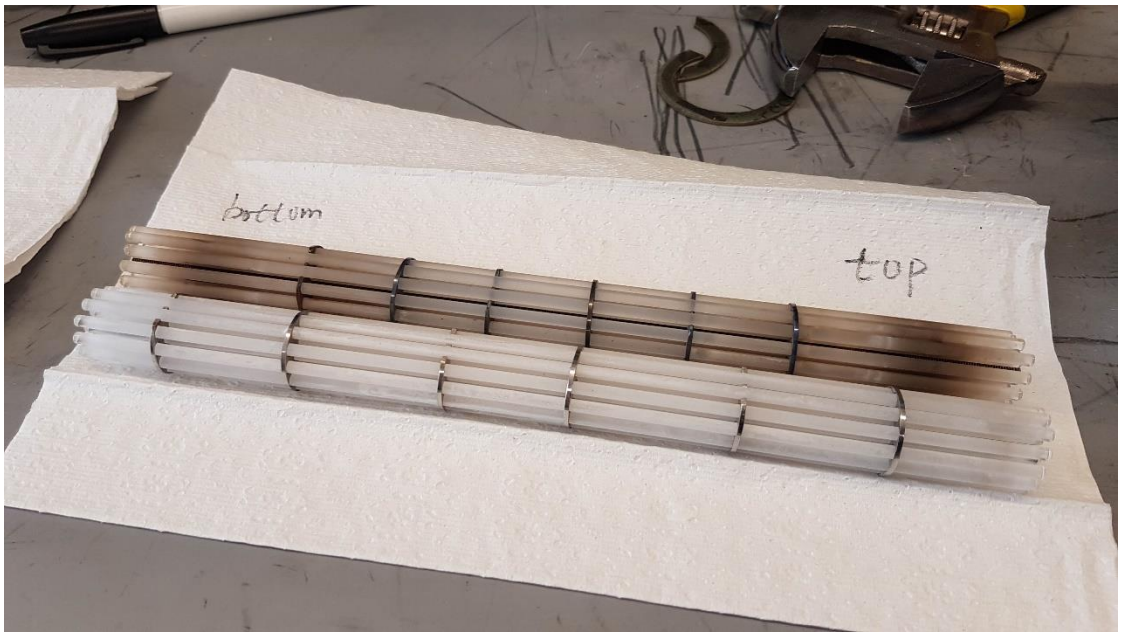

Figure 2.7-3 - Used guidance rods with a light Carbon deposition vs. a newly coated rod.

Summary of experimental conversions results could be seen in **Error! R eference source not found.**, presenting CO conversion as a function of temperature. These values are true for the duel pathway reaction configuration, photocatalysis as well as the thermal only conversion. The CO conversion is measured amount in the output flow vs. the total amount of carbon in output flow.

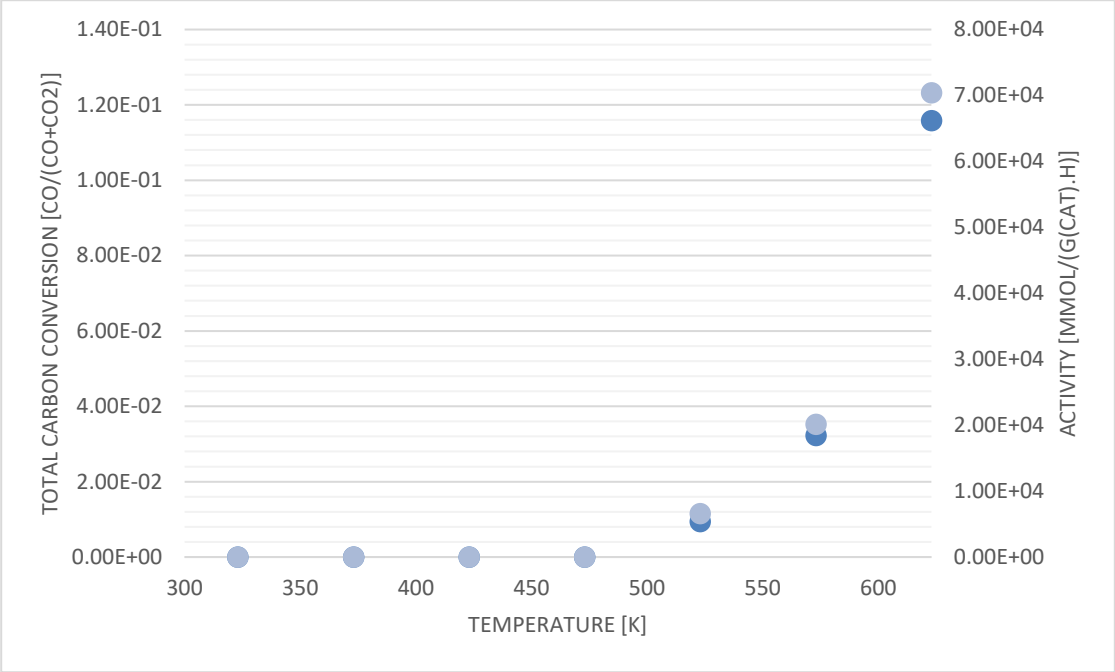

Figure 2.7-4 - Experimental combined total conversion as a function of temperature, including photocatalysis effects.

The results clearly show that reaction in significant amounts starts around the temperature of 500 [K] but increase exponentially. Although this behavior is expected from chemical reactions in general, in this case the increase is better than other reports in the literature. A fitted Arrhenius curve to these results is presented in the next chapter, as it is a calibration tool for the simulations.

SIMULATIONS - COMPUTATIONAL FLUID DINAMICS WITH CHEMISTRY COUPLING MODELING

3.1 Introduction

Numerical calculations and simulations are used in many research operations for several reasons, the most prominent ones are to save time, money and energy by doing predictions to experiments and conditions without practically doing them, which, assuming the simulations' validity, saves a lot of expensive experiments. On other cases simulations help researchers evaluate, learn and understand conditions and boundaries that might not be available in the lab's current capabilities, and in extreme examples simulations could predict unachievable extreme field circumstances. One obvious example is the ability to model scale up sizes of experiments, learning of possible unforeseen challenges that were unobserved in the smaller scale ones. Generally, simulation is a powerful tool for many research and engineering projects, ones it is rigorously calibrated and validated to create a robust and reliable model.

Robust simulation that calculates stable, strong and consistent results depends on initial conditions and parameters as well as the physical models for calculations. Simulations' inputs need to be justified, such as factors that are natural constants or global parameters that should be adopted just as they are,

while others serve as calibration and normalization factors for eliminating numerical errors and upholding all baseline assumptions that were made in the modeling phase.

The simulation tool that was used to simulate these experimental conditions is COMSOL Multiphysics. This program enables to either have several separate physical modules solved to in order to describe the problem, or to have a merge solution that consolidates the different modules in sequential steps or in one consolidated calculation package. The physics modules that were used, in this set of simulations, are linear fluid flow, heat transfer, chemical reaction (1D & 3D), and chemical transport of diluted species. Each of these modules serve a role in the overall representation of the problem, with its physical governing equations, initial and boundary conditions that are paired with an approximation for the existing physical structure.

3.2 First step – Chemical reaction calibration – zero degree of freedom

The first step in simulating the chemical reactor is to understand and define the chemical reaction itself, which is the main product that is compared and

examined throughout the research. The main preferred reaction is the RWGS formula:

$$CO_2 + H_2 \leftrightarrow CO + H_2O$$

As seen in chapter 2.7 – Experimental results, this reaction should reach a theoretical thermal equilibrium of around 18%. In order to describe the reaction most accurately, especially its dependence to temperature and activation energy the Arrhenius equation is naturally chosen:

$$k = A_0 e^{\left(\frac{-E_a}{R \cdot T}\right)}$$

Where:

A_0 is the frequency factor.

E_a is the Activation energy.

$R \cdot T$ is the average kinetic energy.

The use of catalyst inside the reactor and the added photocatalysis aspect of the reaction eliminate the use of theoretical equilibrium conversion as the input parameters for the simulation. In order to calibrate the accurate factors for the Arrhenius equation to accurately describe the chemical reaction an experimental results-based calibration approach was chosen. In this approach actual conversion results from experiments are taken as the base for the conversion and the parameters are achieved by two steps, first, extracting the slope of the natural logarithm of the reaction rate as a function of 1/T as seen

in [**Error! Reference source not found.**] for the activation energy (E_a) and t hen fitting equation-based solutions as seen in Figure 3.2-2 for the frequency factor (A_f).

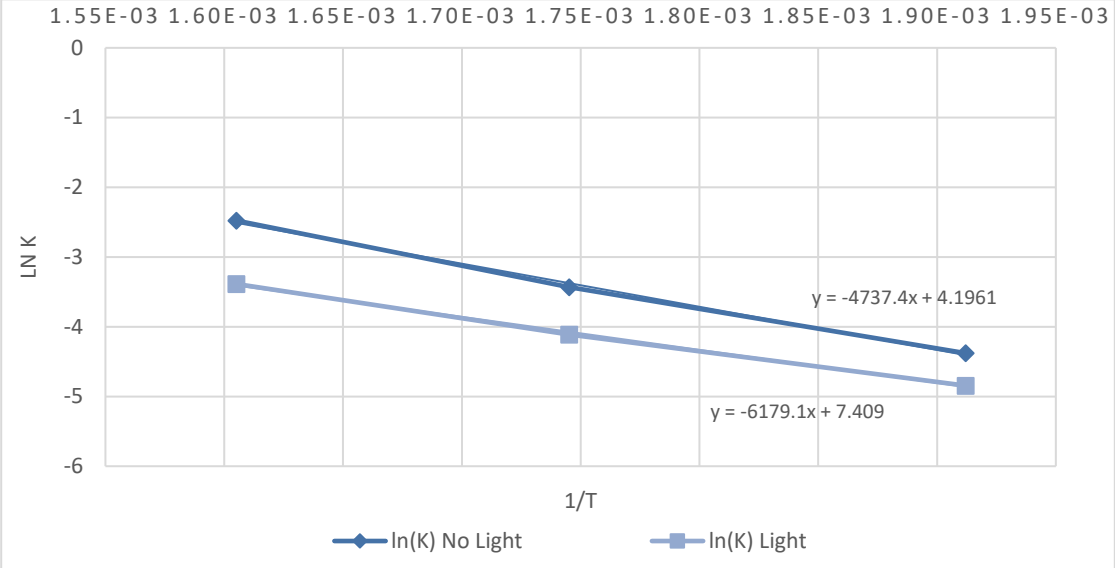

Figure 3.2-1 - Reaction rate logarithmic scale as a function of T-1 for activation energy from the graph's slope.

Table 3.2-1 - Activation energy, taken as the slope values based on experimental results.

	Rounded activation energy
Thermal Only	$13 \cdot 10^3$
Photocatalytic reaction	$5 \cdot 10^3$

The equation for getting the activation energy from the graph's slope:

$$E_a = -R\left[\frac{\partial \ln(k)}{\partial(\frac{1}{T})}\right]$$

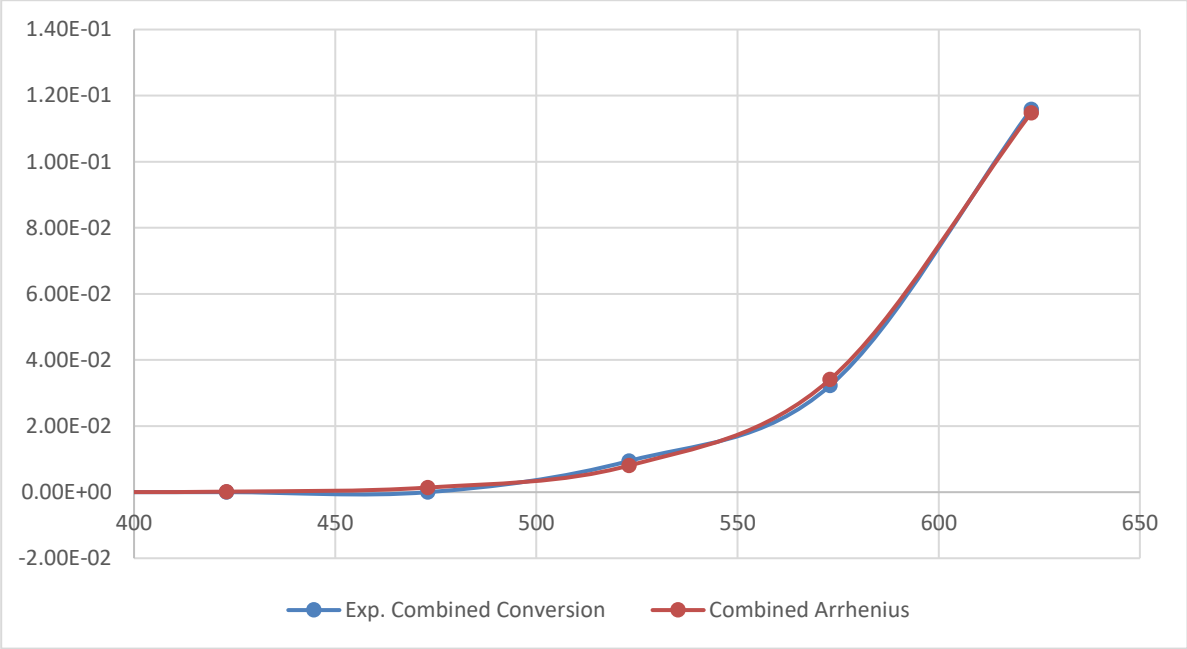

Figure 3.2-2 - Actual Carbon conversion as a function of temperature with the fitted theoretical results of the Arrhenius equation.

Since the reaction inside the reactor is based on the natural thermal equilibrium, but also from the catalytic driven photocatalytic conversion, in the simulation process for this work a two pathways approach was chosen. In order to calibrate two sets of parameters for the two distinct Arrhenius equations the conversion results by temperature were taken, first only the cases without the added use of external light and for the second step the conversion with the added light with the subtraction of the previous results, thus taking the natural thermal effect off out of the combined conversion. By taking this approach it is possible to calibrate two sets of parameters to describe the reactions as seen in Figure 3.2-3.

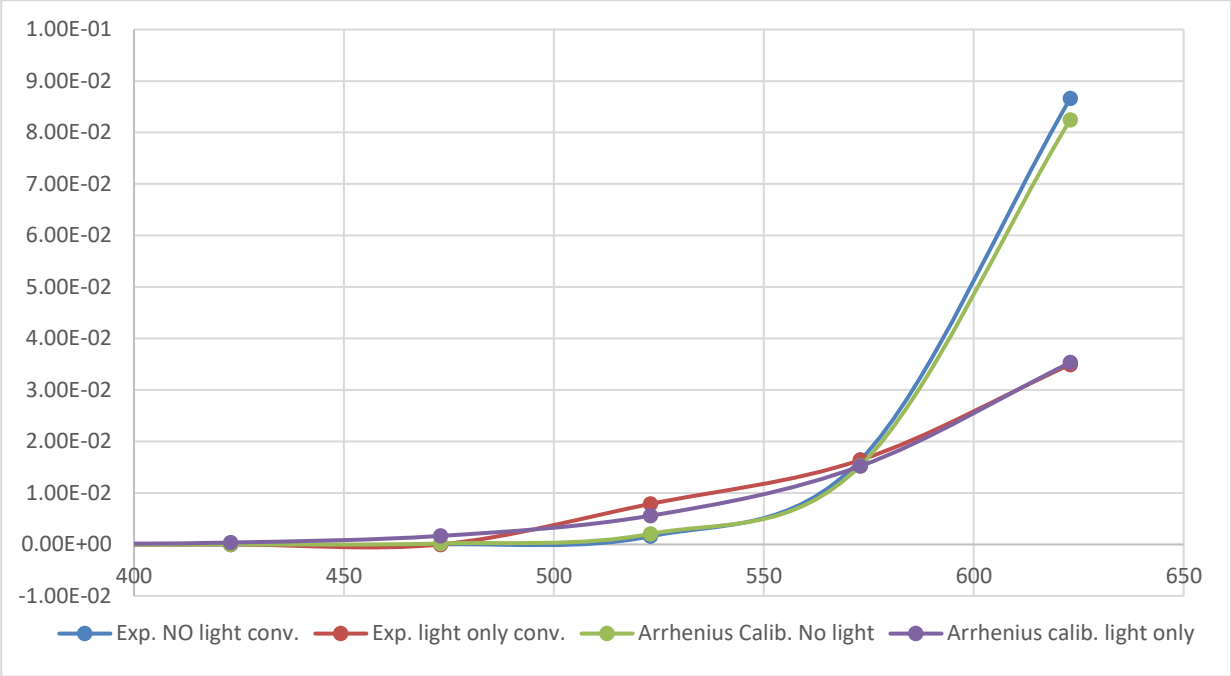

Figure 3.2-3 - Two chemical reaction pathays calibration by fitting theoretical curves on top of experimental results.

Calibration results for the Arrhenius parameters are detailed in Table 3.2-2.

Table 3.2-2 - Arrhenius equation parameters based on experimental results claibration.

	Combined conversion	Thermal conversion – No light	Photochemical component – Light added
Activation Energy – $E_a \left[\frac{kJ}{mol}\right]$	42	60	50

Frequency Factor – $A_0\left[\frac{1}{sec}\right]$	$3.50 \cdot 10^2$	$9 \cdot 10^3$	$5.50 \cdot 10^2$

The reaction rate for the first path, without added light and photocatalytic effect, is based on the Arrhenius conversion factor, concentration of mixed gasses in the reaction and the surface concentration of the catalyst. The second path describes the catalytic attribute to the reaction with the photocatalytic effect, by incorporating different Arrhenius conversion factor, available from the different calibrated parameters, and the emitted light from the guidance rods presented as the light function. These two pathways are described in the following formula representation:

$$r_{No\_Light} = k_{Ar-NL}\frac{[CO_2][H_2]}{[CO][H_2O]} \cdot C_{sur}$$

$$r_{Light} = k_{Ar-L}\frac{[CO_2][H_2]}{[CO][H_2O]} \cdot C_{sur} \cdot Light\ function(X_{rods})$$

The light function is the description for the power source attenuation along the guidance rods. This function will be discussed with detail in the next chapters, since in the zero theoretical representation of the chemical reaction

there is no physical structure to fit the function on, hence, not practical significance.

Both reactions have an equilibrium coefficient that keeps both the reverse and forward, reaction rate complementary to each other, i.e. the forward reaction rate is calculated by the calibrated Arrhenius parameters while the reverse by the inverted forward reaction over the equilibrium constant. Figure 3.2-4 describes the equilibrium conversion change with respect to the reaction temperature.

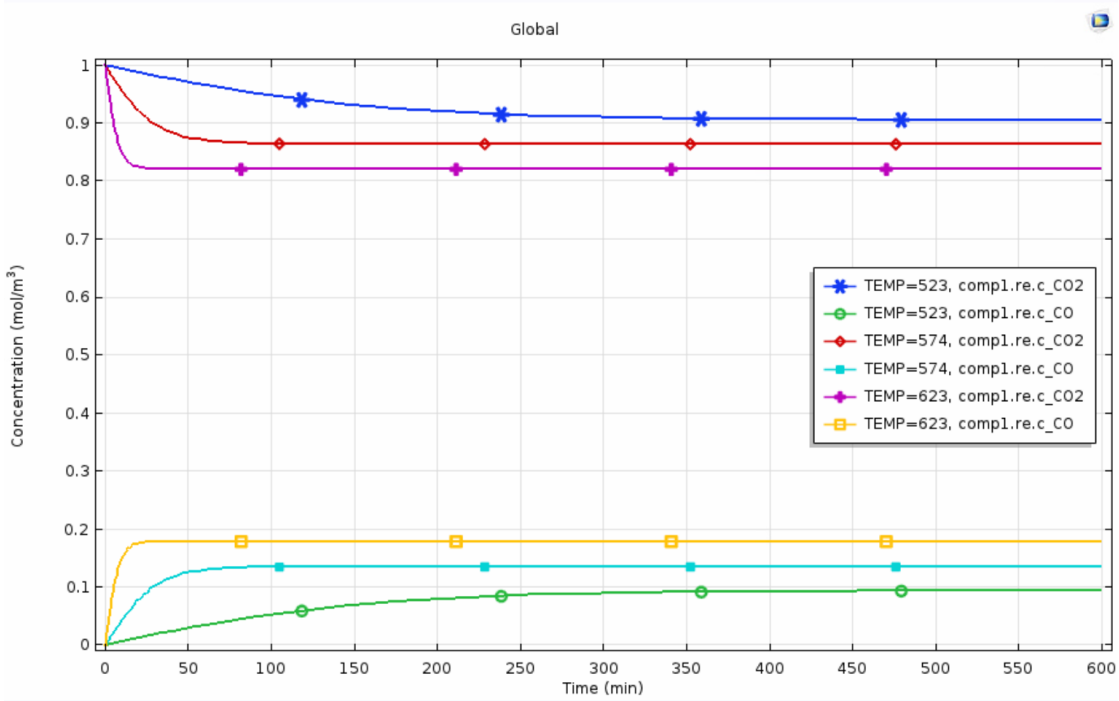

Figure 3.2-4 - Thermal conversion change with respect to different temperatures based solely on thermal catalytic conversion with an added parameter to compensate for the missing photocatalytic reaction.

3.3 Two-dimensional representation for model analysis

The next crucial step to achieve a truthful simulation that accurately describes the physical reactor is to move from the simple time dependent calculation into Multiphysics simulations based on a geometrical model. This step starts with the creation of the best possible two-dimensional representation of the reactor to analyze the calculations on a geometric model, because the reactor could not be accurately described in a simplistic two-dimensional manner some assumptions and accuracy sacrifices had to be made. Figure 3.3-1 is an image taken from the COMSOL program of the latest 2D geometrical representation for the reactor, it is clearly visible that the guiding rods are segmented along the length of the reactor to allow the simulated flow to be as similar as the actual flows as possible. This inaccurate two-dimensional model is important to further calibrate geometrically based parameters, like the light attenuation along the rods, and further analyze the robustness and accuracy of the cupelled Multiphysics modules.

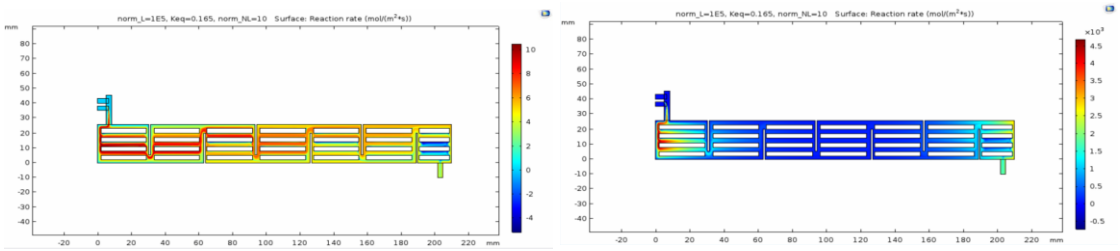

Figure 3.3-1 - Comparison of the two reaction pathways on the 2D reactor's model, thermal only reaction (left) and photocatalysis (right).

Once the geometrical model becomes the base of the simulation the entire Multiphysics cupelled modules approach is being added. Laminar flow solver module is added to account for the gas flow computational fluid dynamics, diluted species module is introduced to solve the dilution, mixture and concentrations of the different gasses, and a chemistry module is added to calculate the chemical reaction behavior of the mixed gases. The last comprised of mostly the same calibrated parameters from the non-dimensional case, with some alteration that will be discussed further on. The calculation of the modules is planned in two stages, the first is the laminar flow solver that calculates the flow inside the reactor solely based on introduced gas flows, which in the second step of the calculation, is cupelled to both the chemical reaction and the diluted species, which are calculated together.

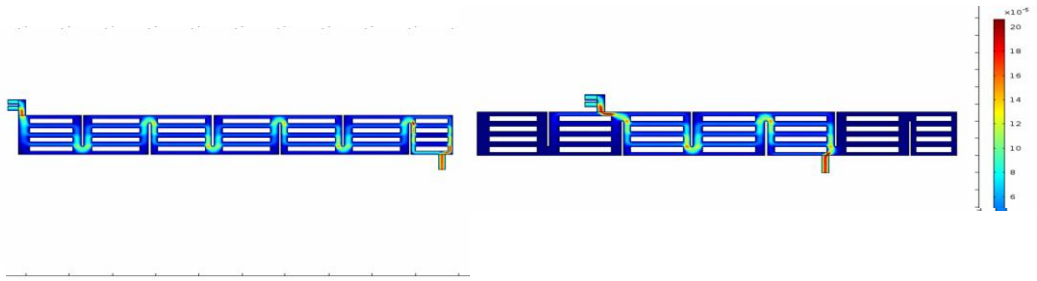

Figure 3.3-2 - Flow comparison of Swagelok components (Right) vs. Customized design ports in an ideal state (Left).

Determination of the characteristic flow regime of the problem is gained by inspecting the flow and physical parameters within the reactor as in Figure 3.3-2 comparing old configuration model based on Swagelok to a costumed built one. Before building the model and using numerical modules, flow characteristics of the gas flow within the reactor is examined. Flow nature, whether laminar or turbulent, is first calculated through the Reynolds number:

$$Re = \frac{\rho u D}{\mu} = \frac{0.559 \cdot 0.025 \cdot 2.54 \cdot 10^{-2}}{3.101 \cdot 10^{-5}} = 11.45$$

Where at atmospheric pressure and temperature of 350°C:

ρ is the density of the gas – $0.559\left[\frac{kg}{m^3}\right]$

u is the velocity of the gas – $0.025\left[\frac{m}{s}\right]$

D is the characteristic length – $2.54 \cdot 10^{-2}[m]$

μ is the dynamic viscosity – $3.101 \cdot 10^{-5}\ \left[\frac{kg}{m \cdot s}\right]$

The calculated Reynolds number value clearly describes a laminar flow state in a pipe, which allows the chosen laminar flow solver to be used as the

CFD solver in this case. The governing equations for the computational laminar flow solver, consisted of the Navier-Stocks equations and the continuity equation:

$$\frac{\partial \rho}{\partial t} + \nabla \cdot (\rho\, \vec{v}) = 0$$

$$\frac{\partial}{\partial t}(\rho\, \vec{v}) + \nabla \cdot (\rho\, \vec{v}\vec{v}) = -\nabla P + \nabla \cdot \mu\left[(\nabla\, \vec{v} + \nabla \vec{v}^{T}) - {}^{2}/_{3}\, \nabla \cdot \vec{v} I\right]$$

The chemical module governing equations are built on the reaction rates:

$$r_j = k_j^f \prod_{i \in Reactants} c_i^{-v_j} - k_j^r \prod_{i \in Products} c_i^{v_{ij}}$$

As seen in the above equation the reaction rate is derived from the multiplication of the gasses concentrations by the Arrhenius equation parameter of the reactants less the products. As seen in chapter 4.2, in order to accurately simulate the internal reactions, a two paths approach was taken. While the thermal only reaction rate is represented in the governing equation above, the second path, for the photocatalysis reaction, includes an extra component that accounts for the light energy along the guiding rods.

$$r_j = Light - Function(x) \cdot \left[k_j^f \prod_{i \in Reactants} c_i^{-v_j} - k_j^r \prod_{i \in Products} c_i^{v_{ij}}\right]$$

The geometrical model enables the implementation of the photocatalytic effects in the calculations with the possibility to add the light power, through the light function, as a boundary condition to the guiding rods. The light function is based on a light attenuation experiment along a rod illuminated on one side by a laser power source, with an assumption that laser sourced light attenuation is similar to the LED power source. Fitting of the exponential decay of the light source on the experimental results is described by the formula:

$$Light - Funcion(x) = P_{in} * e^{(-0.05*(x-5))} + P_{in} * e^{(-0.05*(205-x))}$$

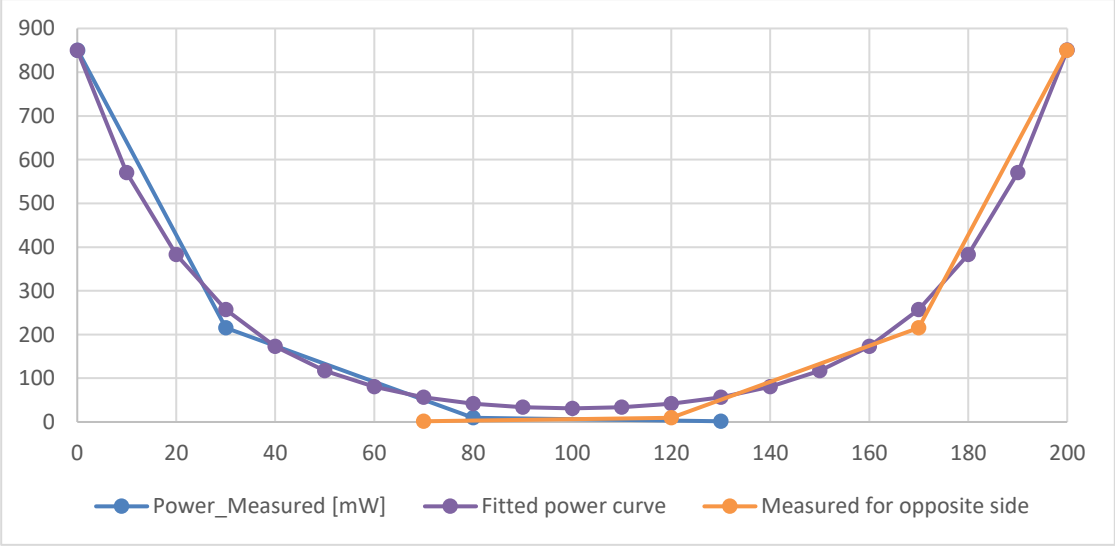

Figure 3.3-3 - Measured light attenuation from both ends of the tested rod with the fitted exponential curve.

The input power source should be normalized to the surface area of a guide rod.

A comparison for the light attenuation was also studied in the model, by checking different input light power and attenuation coefficients, so to imitate a lower decay of light power along the rods. The results and assumptions are described in the results chapter.

Examples for a physical calibrated parameter are the equilibrium constant that sets up the ratio of conversion for the chemical reaction, and for a theoretical one is the change in ratio of reaction from the 1D numerical module to the representative 2D model that have actual catalytic surface ratio to reactor's volume.

3.4 Three-dimensional model

The three-dimensional step is the most accurate representation for the physical photocatalytic reactor. Calibrating the model based on previous experiments and simulation steps allows the robust representation of the complete reaction inside the chemical reactor. Initial model element number was around 6 million, after symmetry assumption was made, which was reduced with mesh optimization to the current number of a little less than $1.5 \cdot 10^6$ elements. This number of elements is not further reduced to refrain from decreased accuracy of results and to make the entire calculation more immune to error values that crashes the calculation.

3.5 Simulations' selected parameters for optimization

The main use of the simulation in this research context, after calibration and during actual lab-experiments, is the general optimization of geometrical properties and physical boundary conditions. Compared attributes were:

- Baffle number
- Baffle height
- Flow rate
- Reactor diameter
- Guiding rods diameter
- Input light intensity
- Decay factor for light attenuation

All comparisons were done in a normalized fashion to the calibrated lab configuration, in order to understand which geometrical changes the greatest impact could have compared to current configuration and in what are the optimal current changes to be made.

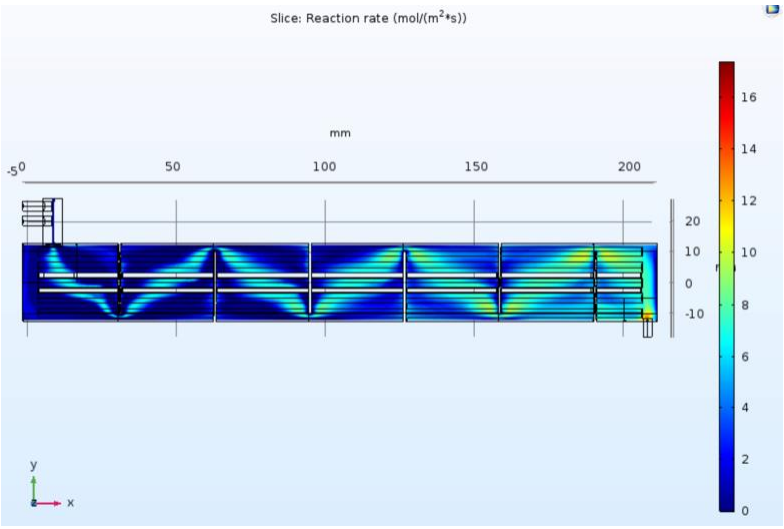

Figure 3.5-1 - Thermal reaction rate across the reactor.

3.6 Analysis

Between the checked parameters, some were easily compared and analyzed in the simulations, while others did not represent any significant difference. The lack of change in some of the parameters is estimated in this section as part of a detailed explanation of changes and implications. One of the easier parameters to change and evaluate is the number of baffles. It is obvious that adding baffles improve the flow mixing with as small price of increased back pressure as seen visually in Figure 3.6-1 and summarize in a graph in Figure 3.6-4.

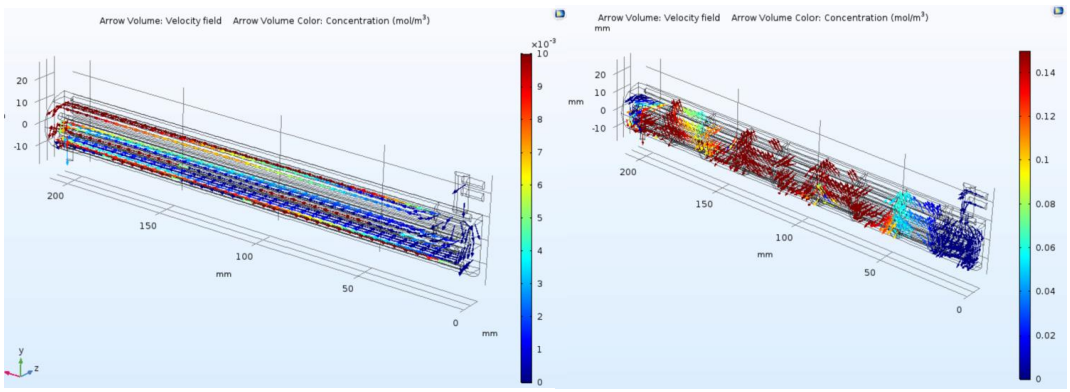

Figure 3.6-1 - Zero baffle and 12 Baffles configuration with arrow plots representing flows and CO concentration.

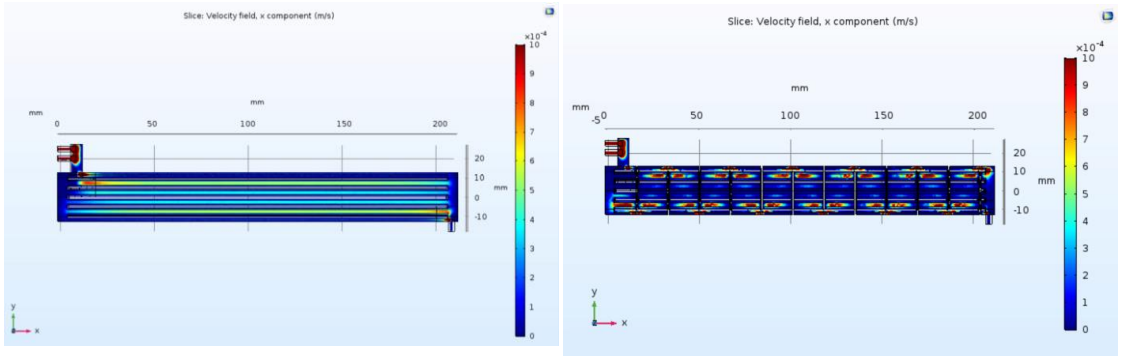

Figure 3.6-2 - Zero and 12 baffles x-direction flow comparison.

The same conclusion could not be made for the overall height of the baffles, since from a certain height not only the flow is almost completely blocked, it also reduces the horizontal opening, making the mixing of the cross section, less optimal in a significant way.

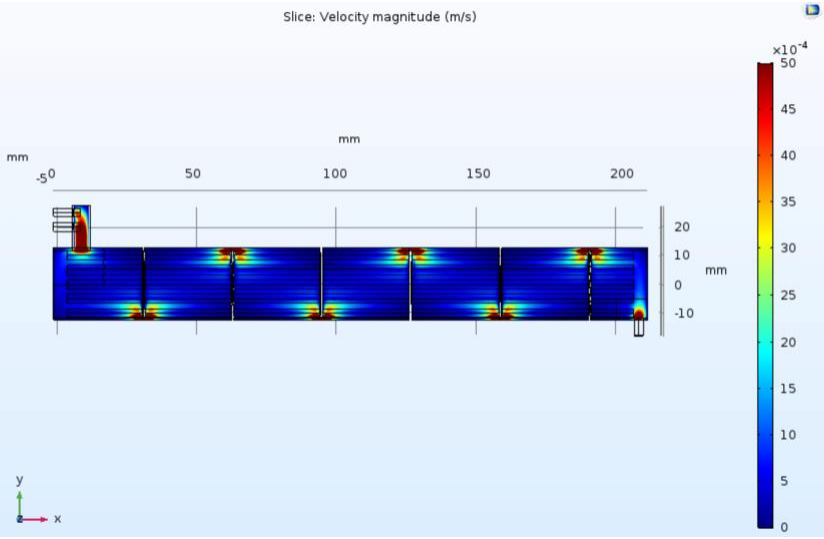

Figure 3.6-3 - Flow field of baffle with 8% height opening.

Lower flow rates obviously increase the total reaction, since they increase retention time, that respectively effects reaction time. In very low flows, there are two main challenges to consider. First and most challenging from a commercial point of view is overall conversion amounts, named activity, that directly depends on flow rates. Second, in the lab-experiments scale, on very low flow rates, every small leak in the reactor or connections, could lead to a massive noise in measured values, due to large fluctuations in reaction comprised gas.

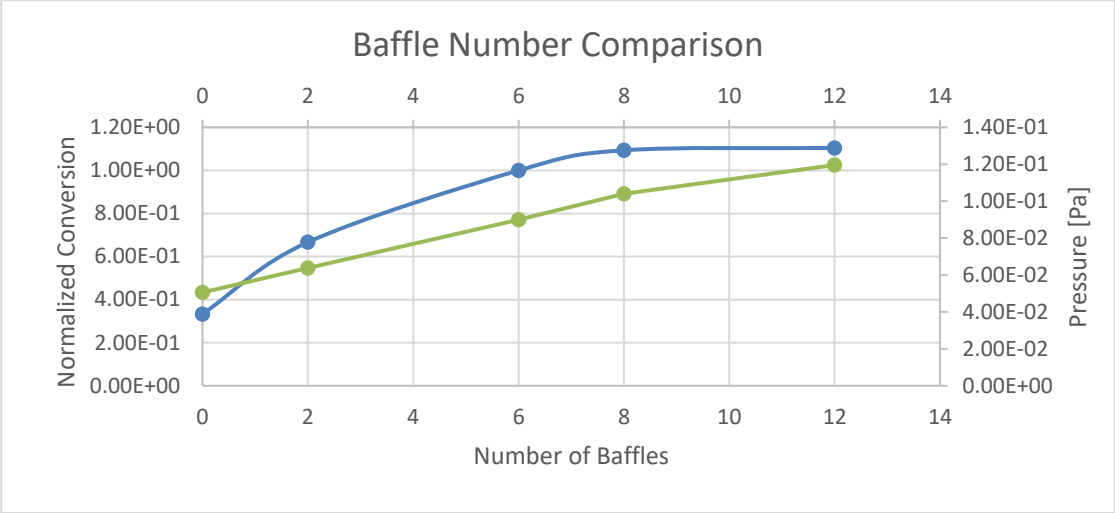

Figure 3.6-4 - Normalized conversion and formed back pressure as a function of number of baffles.

Keeping the same internal volume and increasing reactor diameter, clearly translates to lower light attenuation distance inside the reactor as seen in a numerical calculation in Figure 3.6-5. Lower attenuation directly translates to increased photocatalytic effect, due to increased light on catalyst throughout the length of the reactor. The larger aperture diameter of light that could be introduced to the reactor, also increase the ability for maximum light integration to the reactor. One fact that should be taken into account in the case of a larger diameter reactor experiments, is that a different light source with larger emission area should be used in order to efficiently use to cover the entire 'window' area.

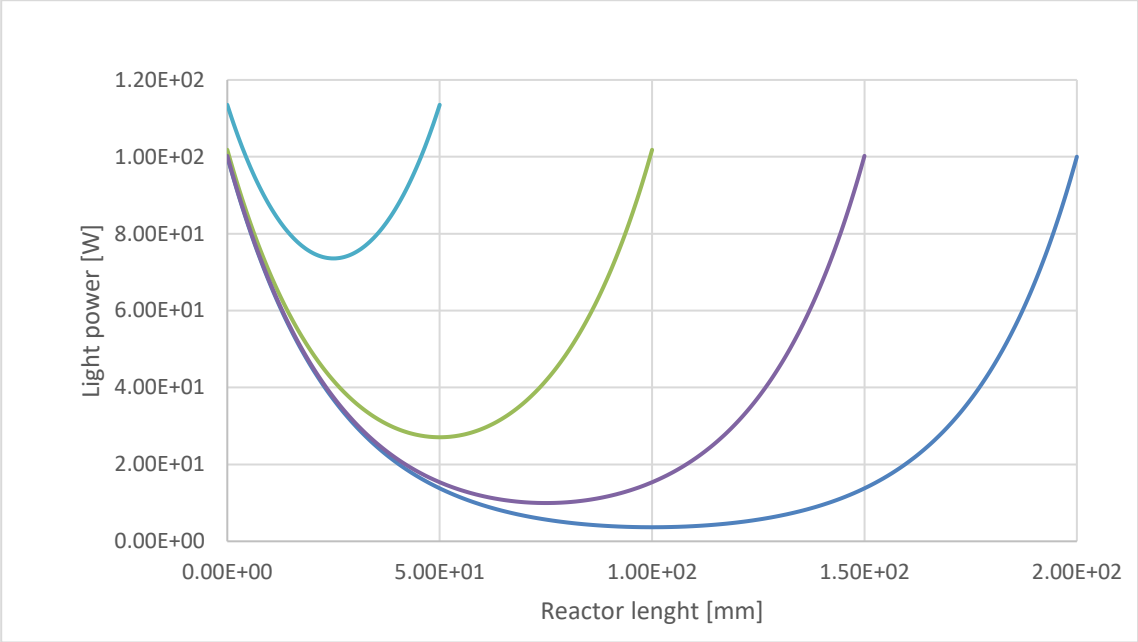

Figure 3.6-5 - Light attenuation as a function of reactor length, considering a 100W input.

Guiding rods diameter, while keeping the same number, is obviously an improvement factor for catalyst surface area ratio against reactor's volume. This immediate insight although physically true, might miss other changed factors, such as mixing flow regime or formed backpressure. These results from current simulation configuration show inconclusive change in output products and should be further calibrated and examined before they could be used as they currently are. This could be handled by testing physical light attenuation along rods with different diameters, since currently, light attenuation equation has no physical parameters dependency to the actual rods, e.g. there is no place for a changed rod diameter to present simulation change, other than flow obstruction.

Another tested parameter is light attenuation for input light along rods' length. In the case of a lower light attenuation due to a different rod physical conditions, i.e. The case of different amounts of sand blasting. As seen in Figure 3.6-6 for a reference input power of 100 [W], as measured in previously described lab experiments, attenuates to almost 0 [W] in the center of a 200[mm] rod that is illuminated from both sides, while in the case of an exponential decay factor which is halved or a rod who's length is only 100 [mm], the minimum power is more than 20 times higher.

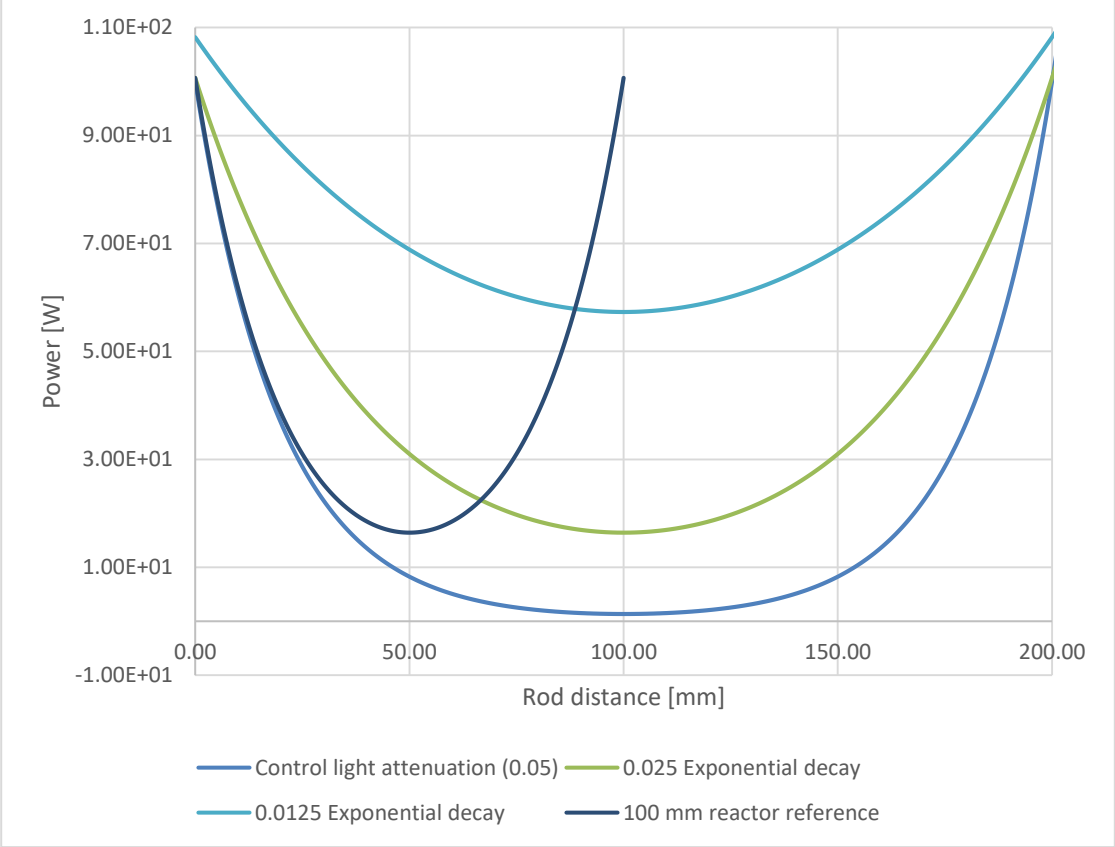

Figure 3.6-6 - Exponential decay factor comparison.

In Figure 3.6-7 the reverse linear connection of the normalized conversion as a function of the exponential decay factor is clearly visible. It can be inferred from the figure that by reducing physical light attenuation, changing rods' physical properties, the photocatalytic reaction will be linearly increased throughout the reactor. Reducing attenuation properties might be done by experimenting different rod diameters or surface roughness might prove highly promoting for the photocatalytic process which will improve the overall conversion.

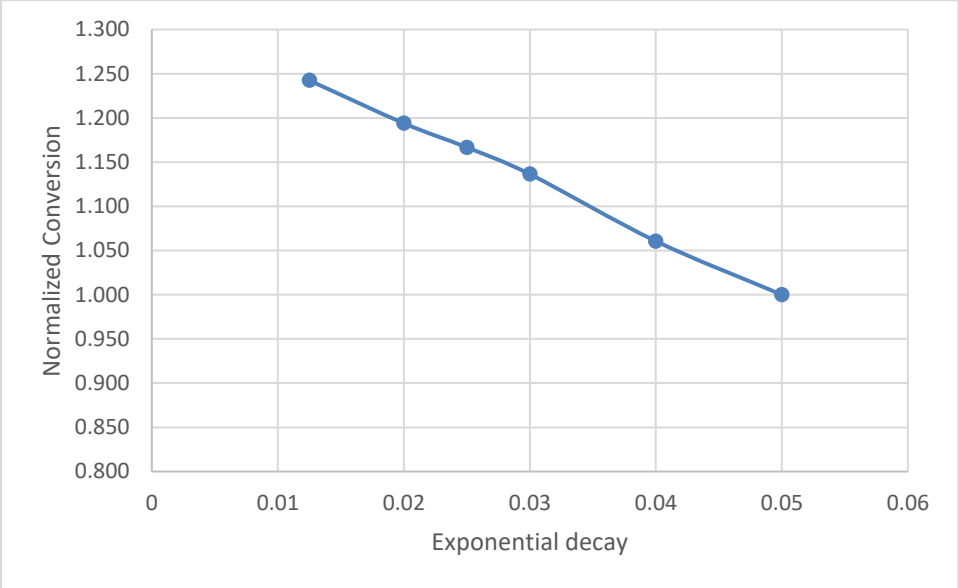

Figure 3.6-7 - Normalized conversion as a function of the exponential decay factor.

It is visible in Figure 3.6-8 that the change in overall photocatalysis reaction, is mainly achieved from the increase of reaction along the reactor's length,

rather than an increase in the peak intensity of the reaction. Mostly higher reaction area is increased along the reactor's length and does not concentrate on the edges of the reactor, as seen in higher decay factor, which as seen before correlates to lower photocatalytic reaction.

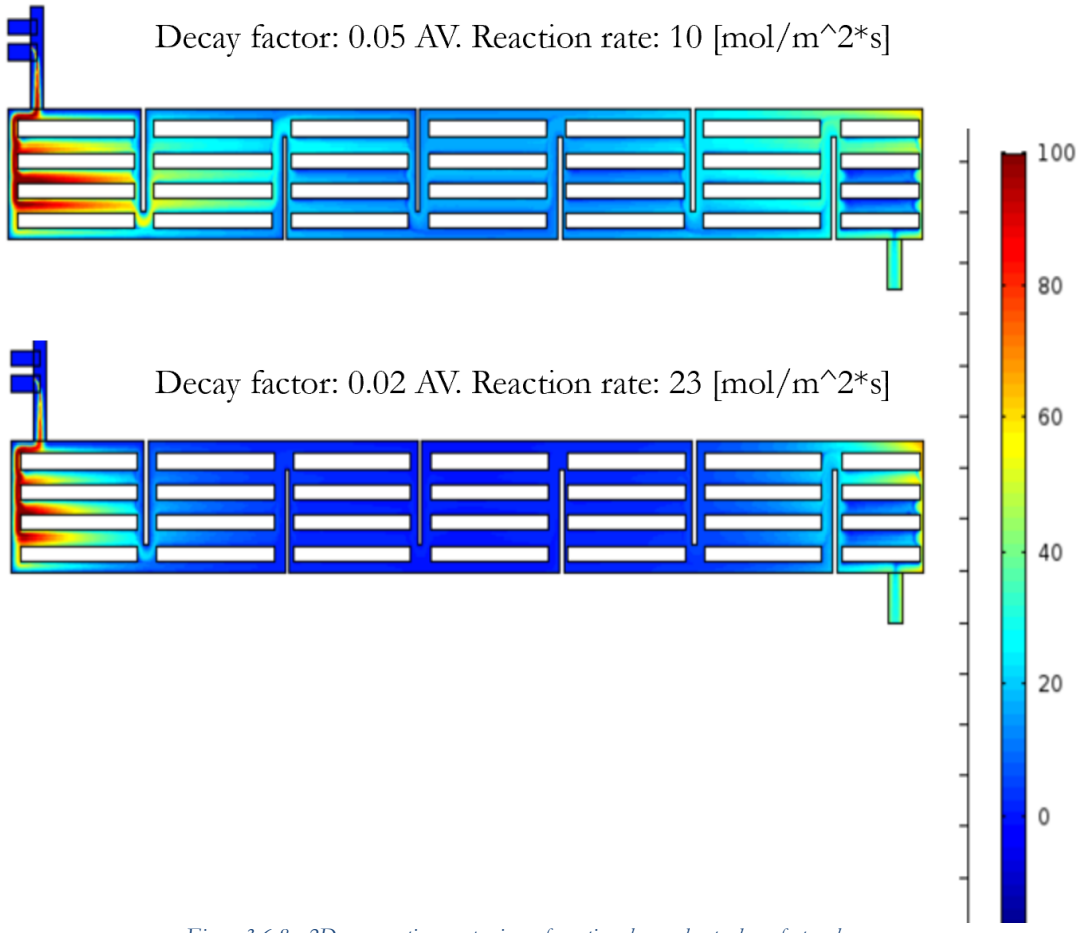

Figure 3.6-8 - 2D cross section comparison of reaction change due to decay factor change.

One case that simulations might not represent well is light source intensity. In simulations, light intensity is linearly connected to the photocatalytic reaction, in real-life different light intensities might push the reaction un-linearly, or

even in the reverse direction. These behaviors which are unknown, are not described in simulation entirely. Light intensity should be studied further outside simulations' analysis frame.

Helical baffle structure

The conceptual internal helical baffle structure has been proposed several times during different experimental stages as the best passive mixing flow configuration possible. Two different configurations were tested numerically, One were the baffles are three quarters full, allowing gas flow only through one quarter in a spiral changing fashion as seen in Figure 3.6-9. Second configuration has one quarter baffles that allow flow through most of the cross section, only slightly diverting the gas directions Figure 3.6-10.

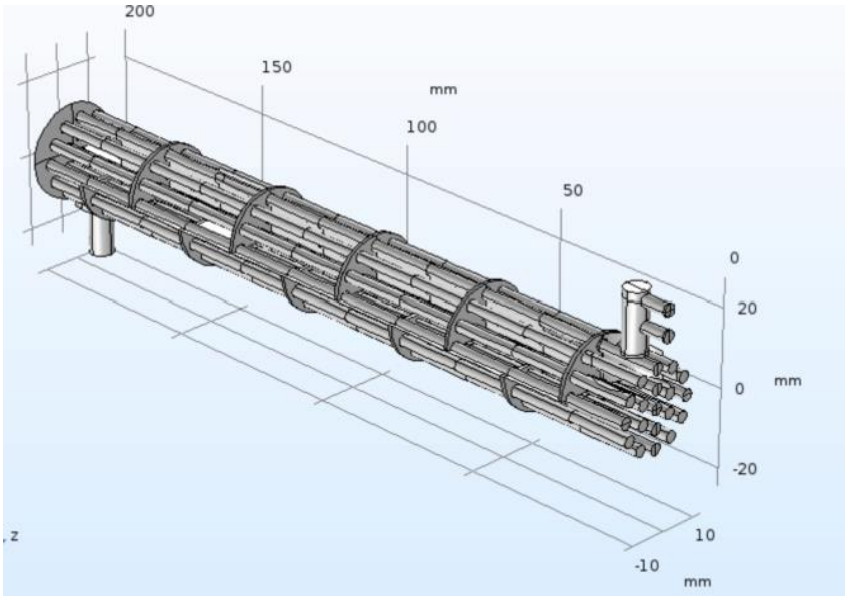

Figure 3.6-9 - First helical baffle configuration.

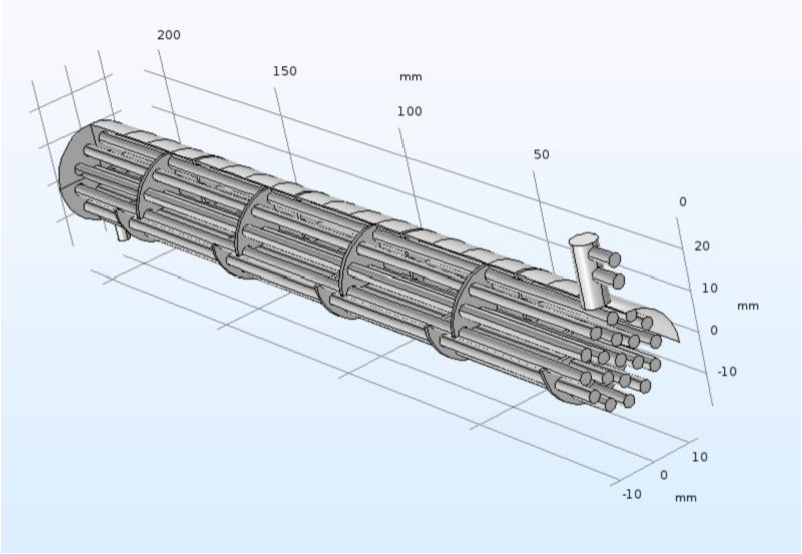

Figure 3.6-10 – Second helical baffle configurations.

The results for the helical shape are inconclusive as seen in Table 3.6-1. Since they only show reduced conversion, especially the ¾ configuration showing slight decrease, that could be explained by numerical conversion, due to large structural changes.

Table 3.6-1 - Helical configuration comparison outcome.

	Conversion	Normalized conversion
Regular 6 baffles	1.44E-1	1
¾ full helical	1.15E-1	0.8
¼ full helical	1.5E-2	0.104

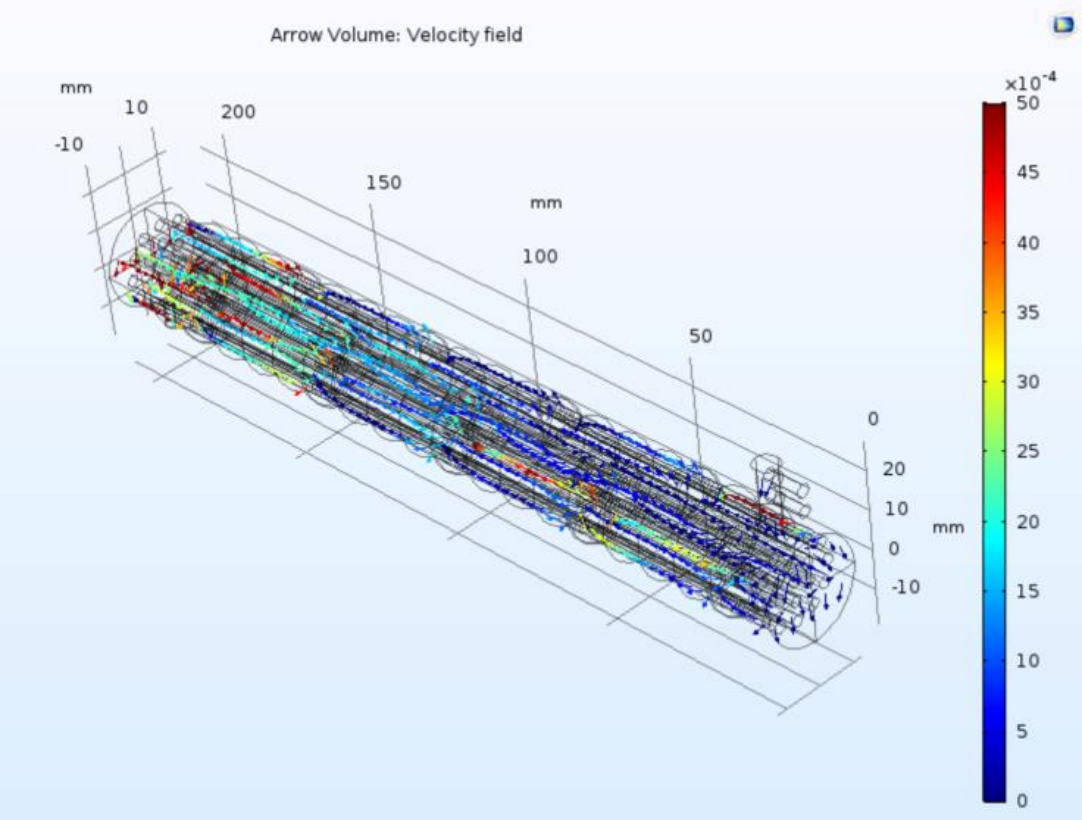

Figure 3.6-11 - 3D representation of the flow and CO increasing concentration in a helical ¼ full reactor.

3.7 Conclusion

In conclusion, simulations have been proven to be a valuable tool to understand and optimize reactor design. Simulations, especially based on a multitude of physical modules, carefully calibrated and rigorously developed can present beneficial information with low cost and effort. While setting up simulations, every parameter should have a physical or experimental meaning, either theoretical to address some component of a physical equation, or a theoretical one for assumptions or limitations of simulations.

Simulations revealed many helpful outcomes, while most insights and optimization analysis were done above, One clear case is that using a shorter thicker reactor, while keeping the same configuration of structure and volume, will improve photocatalysis, because of lowered light attenuation along the length. Another result which was less obvious was that increasing the baffle number slightly, which is an effortless adjustment, could still produce improved outcomes.

DISCUSSION AND CONCLUSIONS

4.1 Future work

Carbon dioxide reduction through photocatalysis, in this research, has presented an interesting potential for conversion percentile and overall conversion amounts. In order to achieve better results and evolve the research, planning a road map is paramount. While some future experiments are necessary to show better research accuracy and system robustness, others, are necessary steps towards advancements. Further proposed steps that could be accomplished are diverse and deal with every aspect of the research. One such example is the transition to a natural light source, to facilitate the plan to use sunlight as the photocatalysis power source, this move could first be accomplished inside the lab by using a sunlight simulator power source that will imitate the sun's natural wavelength spectrum. In parallel to transition to natural sun rays as the power source, the design of a solar collector that will direct enough light beams into the reactor is needed. The size of the sun-rays collector will be determined by calculating the overall power needed to comply with the reaction versus the sun's energy spectrum. Another planned major research direction is evaluating the scalability of the work into industrial size. Understanding and solving the design and operations challenges, scale-up research could be done either through lab experiments, studying new designs,

or through theoretical work using simulations and numerical analysis to evaluate feasibility studies. The scaling up analysis of Carbon sequestration technologies is mandatory due to the size and volume of the problem, and every solution must have an answer in plan.

4.2 Conclusion

This work has introduced the ongoing research project for mitigation solution of the greenhouse gas, Carbon Dioxide, by reduction them into a sin-gas mixture, while presenting high conversion rates. The unique reactor design, that during this work underwent several optimization iterations, grants easy handling, operation and improved light coupling into the chemical chamber as a source for the photocatalytic reaction. The reactor's internal structure of rods and baffles, which was borrowed from the shell and tube heat exchanger, have proven to be a good and easy photochemical reactor idea, both in the aspect of effective gas mixture for better conversion and easy light introduction into deeper sections of the reactor, by light guiding rods. These rods enabled an easy light coupling into the reactor, while also serving as a solid base for catalyst coating. Introducing light into the reactor through the catalyst on the rods, thus ensuring a maximum dispersion, promoting the

photocatalytic effect, but also a spread-out catalytic bed throughout every section of the reactor.

The final chosen catalyst presented high conversion rates, especially high contribution of the photocatalytic conversion path. Despite best efforts and previous contradictive knowledge, it was reviled through the experimental work that the catalyst can be easily deactivated in high temperature (above $300°C$), resulting initially in the elimination of the photocatalytic effects, and later in an overall reduced conversion rates on the thermal path. Future work should include catalyst deactivation charts and an economic conversion calculation to understand the optimal use of the catalyst taking into account the possible necessary replacement.

On the second part of this work, which was done parallel to the experimental work, Computational simulations using COMSOL Multiphysics have helped create a better, easier and cheaper optimization process for both the reaction and reactor. Simulations reveal details that are otherwise unachievable, such as behavior of internal flows or predictions for a large array of experimental conditions that will be expensive and time consuming. Even before the full calibration of the chemical reaction, computational fluid dynamics have allowed a better understanding of the internal flow and mixing of the reactants, thus allowing for an early geometrical iteration step, solely for gas

flow improvements. More generally, once the simulations were calibrated to accurately account for the catalyst behavior and the different paths for the chemical behavior, they were used as a good tool for improving output products. Future work should include a better understanding of the coating thickness of the catalyst on the chemical reaction behavior, which in the simulations is managed through Arrhenius' equation parameters, and may result in additional parameter for the coating of the catalyst, or under the assumption of uniform coating, an added function to the photocatalytic path reaction rate that is directly connected to the catalyst general amount, hence thickness.

Despite infancy challenges both in the simulations and the experimental work, the presented research holds great prospects from achieved results. Presenting research potential to attain in future work, such as increasing conversion rates, improving selectivity of the products and looking not only on the RWGS reaction but other different reactions with more appealing products or more redundant reactants. The motivation to succeed will keep increasing publicly, outside the lab, especially when common interest keeps growing as climate change effects becomes more visible and pronounce. Finding more efficient catalysts and integrating light better into the reactor, enhancing the photocatalytic effect will make it an attractive technology to use as part of the

joint effort for Carbon sequestration. The presented simulations which are based on the problem's physics and calibrated through physical experiments, have helped shed more light on previous behaviors of the system and offered optimization steps to increase the overall conversion. Additional advantage is the ability to predict untested experimental conditions or optimize the design of different system's scales or geometrical structures and their outputs.

REFERENCE

[1] V. Masson-Delmotte, P. Zhai, H. Portner, and D. Roberts, "Intergovernmental Panel on Climate Change. Global Warming of 1.5° C: An IPCC Special Report on the Impacts of Global Warming of 1.5° C Above Pre-industrial Levels and Related Global Greenhouse Gas Emission Pathways, in the Context of Strengthening the Global Response to the Threat of Climate Change, Sustainable Development, and Efforts to Eradicate Poverty." 2018.

[2] J. Artz *et al.*, "Sustainable Conversion of Carbon Dioxide: An Integrated Review of Catalysis and Life Cycle Assessment," *Chem. Rev.*, vol. 118, no. 2, pp. 434–504, Jan. 2018.

[3] P. Zhou and M. Wang, "Carbon dioxide emissions allocation: A review," *Ecol. Econ.*, vol. 125, pp. 47–59, May 2016.

[4] Y. Tan, W. Nookuea, H. Li, E. Thorin, and J. Yan, "Property impacts on Carbon Capture and Storage (CCS) processes: A review," *Energy Convers. Manag.*, vol. 118, pp. 204–222, Jun. 2016.

[5] Y. A. Daza and J. N. Kuhn, "CO $_2$ conversion by reverse water gas shift catalysis: comparison of catalysts, mechanisms and their consequences for CO $_2$ conversion to liquid fuels," *RSC Adv.*, vol. 6, no. 55, pp. 49675–49691, 2016.

[6] C. A. Callaghan, "Kinetics and catalysis of the water-gas-shift reaction: A microkinetic and graph theoretic approach," 2006.

[7] X. Chen *et al.*, "Theoretical Insights and the Corresponding Construction of Supported Metal Catalysts for Highly Selective CO $_2$ to CO Conversion," *ACS Catal.*, vol. 7, no. 7, pp. 4613–4620, Jul. 2017.

[8] J. E. Miller, "Initial case for splitting carbon dioxide to carbon monoxide and oxygen.," SAND2007-8012, 926371, Dec. 2007.

[9] M. Ghoussoub, M. Xia, P. N. Duchesne, D. Segal, and G. Ozin, "Principles of photothermal gas-phase heterogeneous CO 2 catalysis," *Energy Environ. Sci.*, vol. 12, no. 4, pp. 1122–1142, 2019.

[10] W. Hou and S. B. Cronin, "A Review of Surface Plasmon Resonance-Enhanced Photocatalysis," *Adv. Funct. Mater.*, vol. 23, no. 13, pp. 1612–1619, Apr. 2013.

[11] J.-W. Wang, H.-H. Huang, J.-K. Sun, T. Ouyang, D.-C. Zhong, and T.-B. Lu, "Electrocatalytic and Photocatalytic Reduction of CO 2 to CO by Cobalt(II) Tripodal Complexes: Low Overpotentials, High Efficiency and Selectivity," *ChemSusChem*, vol. 11, no. 6, pp. 1025–1031, Mar. 2018.

[12] Z. Jiang *et al.*, "Nature-based catalyst for visible-light-driven photocatalytic CO 2 reduction," *Energy Environ. Sci.*, vol. 11, no. 9, pp. 2382–2389, 2018.

[13] K. Li, X. An, K. H. Park, M. Khraisheh, and J. Tang, "A critical review of CO2 photoconversion: Catalysts and reactors," *Catal. Today*, vol. 224, pp. 3–12, Apr. 2014.

[14] P. A. Alaba, A. Abbas, and W. M. W. Daud, "Insight into catalytic reduction of CO 2 : Catalysis and reactor design," *J. Clean. Prod.*, vol. 140, pp. 1298–1312, Jan. 2017.

[15] Z.-Y. Wang, H.-C. Chou, J. C. S. Wu, D. P. Tsai, and G. Mul, "CO2 photoreduction using NiO/InTaO4 in optical-fiber reactor for renewable energy," *Appl. Catal. Gen.*, vol. 380, no. 1–2, pp. 172–177, May 2010.

[16] K. K. Ghuman, L. B. Hoch, T. E. Wood, C. Mims, C. V. Singh, and G. A. Ozin, "Surface Analogues of Molecular Frustrated Lewis Pairs in

Heterogeneous CO 2 Hydrogenation Catalysis," *ACS Catal.*, vol. 6, no. 9, pp. 5764–5770, Sep. 2016.

[17] L. B. Hoch *et al.*, "Carrier dynamics and the role of surface defects: Designing a photocatalyst for gas-phase CO 2 reduction," *Proc. Natl. Acad. Sci.*, vol. 113, no. 50, pp. E8011–E8020, Dec. 2016.

[18] D. Yucha, G. Kulbir, and P. Radian, "Tailoring Surface Frustrated Lewis Pairs of In2O3−x(OH)y for photocatalytic reduction of CO2.pdf," *Adv. Sci.*, vol. 5, no. No.6, 2016.

[19] E. A. Goldstein and R. E. Mitchell, "Chemical kinetics of copper oxide reduction with carbon monoxide," *Proc. Combust. Inst.*, vol. 33, no. 2, pp. 2803–2810, Jan. 2011.

[20] Q. Bellouard, S. Rodat, S. Abanades, S. Ravel, and P.-É. Frayssines, "Design, simulation and experimental study of a directly-irradiated solar chemical reactor for hydrogen and syngas production from continuous solar-driven wood biomass gasification," *Int. J. Hydrog. Energy*, May 2018.

[21] R. Ma, B. Castro-Dominguez, A. G. Dixon, and Y. H. Ma, "CFD study of heat and mass transfer in ethanol steam reforming in a catalytic membrane reactor," *Int. J. Hydrog. Energy*, vol. 43, no. 15, pp. 7662–7674, Apr. 2018.

[22] S. Bellan, N. Gokon, K. Matsubara, H. S. Cho, and T. Kodama, "Numerical and experimental study on granular flow and heat transfer characteristics of directly-irradiated fluidized bed reactor for solar gasification," *Int. J. Hydrog. Energy*, vol. 43, no. 34, pp. 16443–16457, Aug. 2018.

[23] T. Osaki, N. Narita, T. Horiuchi, T. Sugiyama, H. Masuda, and K. Suzuki, "Kinetics of reverse water gas shift (RWGS) reaction on metal disulfide catalysts," *J. Mol. Catal. Chem.*, vol. 125, no. 1, pp. 63–71, 1997.

[24] "1" NPT fused quartz sealed into Stainless 316 housing." .

[25] "Transparent Material Comparison," *Rayotec Scientific Inc.* .

[26] H. Le, T. Wood, and G. A. Ozin, "Spatial separation of charge carriers in In2O3−x(OH)y Nanocrystal Superstructures for photocatalytic activity," *ACSNANO*, 2016.

[27] J. . Smith and H. Van Ness, "Introduction to chemical engineering thermodynamics," in *Effects of temp on equilibrium - chart from intro to chemical thermo.pdf*, 8th edition., Mc Graw Hill, 2018, p. 493.